[4] A. Bikfalvi, S. Klein, G. Pintucci, D.B. Rifkin, Biological roles of fibroblast growth factor-2, Endocr. Rev. 18 (1997) 26–45.
[5] A. Bjorklund, Ö. Lindvall, Chemical Neuroanatomy: Classical Transmitters in the CNS, Elsevier, Amsterdam, 1984.
[6] T.C. Burazin, A.L. Gundlach, Localization of GDNF/neurturin receptor (c-ret, GFRalpha-1 and alpha-2) mRNAs in postnatal rat brain: differential regional and temporal expression in hippocampus, cortex and cerebellum, Mol. Brain Res. 73 (1999) 151–171.
[7] F. Canzian, T. Ushijima, M. Nagao, I. Matera, G. Romeo, I. Ceccherini, Genetic mapping of the RET protooncogene on rat chromosome 4, Mamm. Genome 6 (1995) 433–435.
[8] A.C. Chen, A.J. Eisch, N. Sakai, M. Takahashi, E.J. Nestler, R.S. Duman, Regulation of GFRalpha-1 and GFRalpha-2 mRNAs in rat brain by electroconvulsive seizure, Synapse 39 (2001) 42–50.
[9] K. Chergui, P.J. Charlety, H. Akaoka, C.F. Saunier, J.L. Brunet, M. Buda, T.H. Svensson, G. Chovet, Tonic activation of NMDA receptors causes spontaneous burst discharge of rat midbrain dopamine neurons in vivo, Eur. J. Neurosci. 5 (1993) 137–144.
[10] A.Y. Deutch, The regulation of subcortical dopamine systems by the prefrontal cortex: interactions of central dopamine systems and the pathogenesis of schizophrenia, J. Neural. Transm., Suppl. 36 (1992) 61–89.
[11] A.Y. Deutch, S.Y. Tam, A.S. Freeman, M.B. Bowers Jr., R.H. Roth, Mesolimbic and mesocortical dopamine activation induced by phencyclidine: contrasting pattern to striatal response, Eur. J. Pharmacol. 134 (1987) 257–264.
[12] P. Durbec, C.V. Marcos-Gutierrez, C. Kilkenny, M. Grigoriou, K. Wartiowaara, P. Suvanto, D. Smith, B. Ponder, F. Costantini, M. Saarma, et al., GDNF signalling through the Ret receptor tyrosine kinase, Nature 381 (1996) 789–793.
[13] G. Ellison, The *N*-methyl-D-aspartate antagonists phencyclidine, ketamine and dizocilpine as both behavioral and anatomical models of the dementias, Brain Res. Rev. 20 (1995) 250–267.
[14] E.D. French, Effects of phencyclidine on ventral tegmental A10 dopamine neurons in the rat, Neuropharmacology 25 (1986) 241–248.
[15] C.M. Gall, S.J. Gold, P.J. Isackson, K.B. Seroogy, Brain-derived neurotrophic factor and neurotrophin 3 mRNA are expressed in ventral midbrain regions containing dopaminergic neurons, Mol. Cell. Neurosci. 3 (1992) 56–63.
[16] D.M. Gash, Z. Zhang, A. Ovadia, W.A. Cass, A. Yi, L. Simmerman, D. Russell, D. Martin, P.A. Lapchak, F. Collins, B.J. Hoffer, G.A. Gerhardt, Functional recovery in parkinsonian monkeys treated with GDNF, Nature 380 (1996) 252–255.
[17] T.G. Hastings, D.A. Lewis, M.J. Zigmond, Role of oxidation in the neurotoxic effects of intrastriatal dopamine injections, Proc. Natl. Acad. Sci. U. S. A. 93 (1996) 1956–1961.
[18] P. Hertel, J.M. Mathe, G.G. Nomikos, M. Iurlo, A.A. Mathe, T.H. Svensson, Effects of D-amphetamine and phencyclidine on behavior and extracellular concentrations of neurotensin and dopamine in the ventral striatum and the medial prefrontal cortex of the rat, Behav. Brain Res. 72 (1995) 103–114.
[19] H. Hondo, Y. Yonezawa, T. Nakahara, K. Nakamura, M. Hirano, H. Uchimura, N. Tashiro, Effect of phencyclidine on dopamine release in the rat prefrontal cortex; an in vivo microdialysis study, Brain Res. 633 (1994) 337–342.
[20] C. Humpel, B. Hoffer, I. Stromberg, S. Bektesh, F. Collins, L. Olson, Neurons of the hippocampal formation express glial cell line-derived neurotrophic factor messenger RNA in response to kainate-induced excitation, Neuroscience 59 (1994) 791–795.
[21] D.C. Javitt, S.R. Zukin, Recent advances in the phencyclidine model of schizophrenia, Am. J. Psychiatry 148 (1991) 1301–1308.
[22] J.D. Jentsch, D.E. Redmond Jr., J.D. Elsworth, J.R. Taylor, K.D. Youngren, R.H. Roth, Enduring cognitive deficits and cortical dopamine dysfunction in monkeys after long-term administration of phencyclidine, Science 277 (1997) 953–955.
[23] S. Jing, D. Wen, Y. Yu, P.L. Holst, Y. Luo, M. Fang, R. Tamir, L. Antonio, Z. Hu, R. Cupples, J.C. Louis, S. Hu, B.W. Altrock, G.M. Fox, GDNF-induced activation of the ret protein tyrosine kinase is mediated by GDNFR-alpha, a novel receptor for GDNF, Cell 85 (1996) 1113–1124.
[24] S. Jing, Y. Yu, M. Fang, Z. Hu, P.L. Holst, T. Boone, J. Delaney, H. Schultz, R. Zhou, G.M. Fox, GFRalpha-2 and GFRalpha-3 are two new receptors for ligands of the GDNF family, J. Biol. Chem. 272 (1997) 33111–33117.
[25] C.M. Kearns, D.M. Gash, GDNF protects nigral dopamine neurons against 6-hydroxydopamine in vivo, Brain Res. 672 (1995) 104–111.
[26] L.F. Lin, D.H. Doherty, J.D. Lile, S. Bektesh, F. Collins, GDNF: a glial cell line-derived neurotrophic factor for midbrain dopaminergic neurons, Science 260 (1993) 1130–1132.
[27] D. Lozovsky, C.F. Saller, M.A. Bayorh, C.C. Chiueh, K.C. Rice, T.R. Burke Jr., I.J. Kopin, Effects of phencyclidine on rat prolactin, dopamine receptor and locomotor activity, Life Sci. 32 (1983) 2725–2731.
[28] S. Marco, J. Saura, E. Perez-Navarro, M. Jose Marti, E. Tolosa, J. Alberch, Regulation of c-Ret, GFRalpha1, and GFRalpha2 in the substantia nigra pars compacta in a rat model of Parkinson's disease, J. Neurobiol. 52 (2002) 343–351.
[29] J.M. Mathe, G.G. Nomikos, B. Schilstrom, T.H. Svensson, Non-NMDA excitatory amino acid receptors in the ventral tegmental area mediate systemic dizocilpine (MK-801) induced hyperlocomotion and dopamine release in the nucleus accumbens, J. Neurosci. Res. 51 (1998) 583–592.
[30] E. Mayer, S.B. Dunnett, R. Pellitteri, J.W. Fawcett, Basic fibroblast growth factor promotes the survival of embryonic ventral mesencephalic dopaminergic neurons: I. Effects in vitro, Neuroscience 56 (1993) 379–388.
[31] I.J. Mitchell, A.J. Cooper, M.R. Griffiths, D.J. Barber, Phencyclidine and corticosteroids induce apoptosis of a subpopulation of striatal neurons: a neural substrate for psychosis? Neuroscience 84 (1998) 489–501.
[32] K. Nishijima, A. Kashiwa, A. Hashimoto, H. Iwama, A. Umino, T. Nishikawa, Differential effects of phencyclidine and methamphetamine on dopamine metabolism in rat frontal cortex and striatum as revealed by in vivo dialysis, Synapse 22 (1996) 304–312.
[33] C.A. Nosrat, A. Tomac, B.J. Hoffer, L. Olson, Cellular and developmental patterns of expression of Ret and glial cell line-derived neurotrophic factor receptor alpha mRNAs, Exp. Brain Res. 115 (1997) 410–422.
[34] J.W. Olney, J. Labruyere, G. Wang, D.F. Wozniak, M.T. Price, M.A. Sesma, NMDA antagonist neurotoxicity: mechanism and prevention, Science 254 (1991) 1515–1518.
[35] D. Otto, K. Unsicker, Basic FGF reverses chemical and morphological deficits in the nigrostriatal system of MPTP-treated mice, J. Neurosci. 10 (1990) 1912–1921.
[36] M. Paquet, M. Tremblay, J.J. Soghomonian, Y. Smith, AMPA and NMDA glutamate receptor subunits in midbrain dopaminergic neurons in the squirrel monkey: an immunohistochemical and in situ hybridization study, J. Neurosci. 17 (1997) 1377–1396.
[37] L. Pawlowski, J.M. Mathe, T.H. Svensson, Phencyclidine activates rat A10 dopamine neurons but reduces burst activity and causes regularization of firing, Acta Physiol. Scand. 139 (1990) 529–530.
[38] G. Paxinos, C. Watson, The Rat Brain in Stereotaxic Coordinates, 4th edition, Academic Press, San Diego, 1998.
[39] N.A. Pochon, A. Menoud, J.L. Tseng, A.D. Zurn, P. Aebischer, Neuronal GDNF expression in the adult rat nervous system identified by in situ hybridization, Eur. J. Neurosci. 9 (1997) 463–471.
[40] R. Quirion, M.A. Bayorh, R.L. Zerbe, C.B. Pert, Chronic phencyclidine treatment decreases phencyclidine and dopamine receptors in rat brain, Pharmacol. Biochem. Behav. 17 (1982) 699–702.
[41] M. Reeben, A. Laurikainen, J.O. Hiltunen, E. Castren, M. Saarma, The messenger RNAs for both glial cell line-derived neurotrophic factor receptors, c-ret and GDNFRalpha, are induced in the rat brain in response to kainate-induced excitation, Neuroscience 83 (1998) 151–159.

[42] H.A. Robertson, Chronic phencyclidine, like amphetamine, produces a decrease in [3H]spiroperidol binding in rat striatum, Eur. J. Pharmacol. 78 (1982) 363–365.
[43] C. Rosenblad, D. Kirik, B. Devaux, B. Moffat, H.S. Phillips, A. Bjorklund, Protection and regeneration of nigral dopaminergic neurons by neurturin or GDNF in a partial lesion model of Parkinson's disease after administration into the striatum or the lateral ventricle, Eur. J. Neurosci. 11 (1999) 1554–1566.
[44] A. Sarabi, B.J. Hoffer, L. Olson, M. Morales, GFRalpha-1 mRNA in dopaminergic and nondopaminergic neurons in the substantia nigra and ventral tegmental area, J. Comp. Neurol. 441 (2001) 106–117.
[45] D.G. Schaar, B.A. Sieber, C.F. Dreyfus, I.B. Black, Regional and cell-specific expression of GDNF in rat brain, Exp. Neurol. 124 (1993) 368–371.
[46] R. Schmidt-Kastner, A. Tomac, B. Hoffer, S. Bektesh, B. Rosenzweig, L. Olson, Glial cell-line derived neurotrophic factor (GDNF) mRNA upregulation in striatum and cortical areas after pilocarpine-induced status epilepticus in rats, Mol. Brain Res. 26 (1994) 325–330.
[47] J. Semba, H. Watanabe, T. Suhara, N. Akanuma, Chronic lithium chloride injection increases glucocorticoid receptor but not mineralocorticoid receptor mRNA expression in rat brain, Neurosci. Res. 38 (2000) 313–319.
[48] J. Semba, N. Tanaka, M. Wakuta, T. Suhara, Neonatal phencyclidine treatment selectively attenuates mesolimbic dopamine function in adult rats as revealed by methamphetamine-induced behavior and c-fos mRNA expression in the brain, Synapse 40 (2001) 11–18.
[49] S. Shimasaki, N. Emoto, A. Koba, M. Mercado, F. Shibata, K. Cooksey, A. Baird, N. Ling, Complementary DNA cloning and sequencing of rat ovarian basic fibroblast growth factor and tissue distribution study of its mRNA, Biochem. Biophys. Res. Commun. 157 (1988) 256–263.
[50] T. Shinkai, L. Zhang, S.A. Mathias, G.S. Roth, Dopamine induces apoptosis in cultured rat striatal neurons; possible mechanism of D2-dopamine receptor neuron loss during aging, J. Neurosci. Res. 47 (1997) 393–399.
[51] I. Stromberg, L. Bjorklund, M. Johansson, A. Tomac, F. Collins, L. Olson, B. Hoffer, C. Humpel, Glial cell line-derived neurotrophic factor is expressed in the developing but not adult striatum and stimulates developing dopamine neurons in vivo, Exp. Neurol. 124 (1993) 401–412.
[52] A. Tomac, E. Lindqvist, L.F. Lin, S.O. Ogren, D. Young, B.J. Hoffer, L. Olson, Protection and repair of the nigrostriatal dopaminergic system by GDNF in vivo, Nature 373 (1995) 335–339.
[53] A. Tomac, J. Widenfalk, L.F. Lin, T. Kohno, T. Ebendal, B.J. Hoffer, L. Olson, Retrograde axonal transport of glial cell line-derived neurotrophic factor in the adult nigrostriatal system suggests a trophic role in the adult, Proc. Natl. Acad. Sci. U. S. A. 92 (1995) 8274–8278.
[54] M. Trupp, E. Arenas, M. Fainzilber, A.S. Nilsson, B.A. Sieber, M. Grigoriou, C. Kilkenny, E. Salazar-Grueso, V. Pachnis, U. Arumae, Functional receptor for GDNF encoded by the c-ret proto-oncogene, Nature 381 (1996) 785–789.
[55] M. Trupp, N. Belluardo, H. Funakoshi, C.F. Ibanez, Complementary and overlapping expression of glial cell line-derived neurotrophic factor (GDNF), c-ret proto-oncogene, and GDNF receptor-alpha indicates multiple mechanisms of trophic actions in the adult rat CNS, J. Neurosci. 17 (1997) 3554–3567.
[56] T. Wang, E.D. French, NMDA, kainate, and AMPA depolarize non-dopamine neurons in the rat ventral tegmentum, Brain Res. Bull. 36 (1995) 39–43.

ELSEVIER

Neuroscience Letters 363 (2004) 33–37

Neuroscience Letters

www.elsevier.com/locate/neulet

Isolation and transplantation of dopaminergic neurons generated from mouse embryonic stem cells

Takahito Yoshizaki[a,b,c], Motoki Inaji[d,g], Hiroko Kouike[a,c], Takuya Shimazaki[a,c], Kazunobu Sawamoto[a,c], Kiyoshi Ando[d,e], Isao Date[h], Kazuto Kobayashi[f], Tetsuya Suhara[d], Yasuo Uchiyama[b], Hideyuki Okano[a,c,*]

[a] *Department of Physiology, Keio University School of Medicine, Tokyo 160-8582, Japan*
[b] *Department of Cell Biology and Neuroscience, Osaka University Graduate School of Medicine, Osaka 565-0852, Japan*
[c] *Japan Science and Technology Agency, Core Research for Evolutional Science and Technology, Tokyo, Japan*
[d] *National Institute of Radiological Sciences, Chiba 263-8555, Japan*
[e] *Central Institute for Experimental Animals, Kanagawa 216-0001, Japan*
[f] *Department of Molecular Genetics, Institute of Biomedical Sciences, Fukushima Medical University School of Medicine, Fukushima 960-1295, Japan*
[g] *Department of Neurosurgery, Tokyo Medical and Dental University, Tokyo 113-8519, Japan*
[h] *Department of Neurological Surgery, Okayama University Graduate School of Medicine and Dentistry, Okayama 700-8530, Japan*

Received 16 January 2004; received in revised form 11 March 2004; accepted 12 March 2004

Abstract

Embryonic stem (ES) cells differentiate into dopamine (DA)-producing neurons when co-cultured with PA6 stromal cells, but the resulting cultures contain a variety of unidentified cells. In order to label live DA neurons in mixed populations, we introduced a GFP reporter under the control of the tyrosine hydroxylase (TH) gene promoter into ES cells. GFP expression was observed in TH-immunoreactive cells that differentiated from the ES cells that carried the *TH-GFP*reporter gene. DA neurons expressing GFP were sorted from the mixed cell population by fluorescence-activated cell sorting of cells exhibiting GFP fluorescence, and the sorted GFP^+ cells obtained were transplanted into a rat model of Parkinson's disease. Some of these cells survived and innervated the host striatum, resulting in a partial recovery from parkinsonian behavioral defects. This strategy of isolation and transplantation of ES-cell-derived DA neurons should be useful for cellular and molecular studies of DA neurons and for clinical application in the treatment of Parkinson's disease.

Keywords: Embryonic stem cells; Dopamine neuron; Transplantation; Stromal-cell derived inducing activity (SDIA); *TH-GFP*

Most of the symptoms of Parkinson's disease are caused by degeneration of dopamine (DA)-producing neurons in the substantia nigra [13], and intrastriatal grafting of DA neurons or their precursors has been reported to ameliorate the motor symptoms of patients with Parkinson's disease [10,16,20]. Although transplantation is considered a promising means of therapy, its clinical use is still restricted to only a few cases. The major factors limiting this therapy are the difficulty of obtaining sufficient donor cells and the controversial ethical and legal issues raised by the use of human fetal allografts [2,5], and as a result, a variety of strategies to generate DA neurons in vitro have been proposed to overcome these problems [3,4]. Techniques that convert neural progenitor cells into DA neurons after expansion of the population in vitro have been reported [8, 17], and protocols to induce DA neuronal differentiation from embryonic stem (ES) cells have also been reported [6, 7,9]. Because neural stem cells and ES cells can be easily expanded in vitro, these approaches seem capable of solving the problems mentioned above. ES cells, in particular, can be expected to provide an unlimited supply of donor source because of their unlimited capacity for self-renewal, but since after their induction the DA neurons generated in vitro exist within a mixed population, which may contain a variety of unidentified cells that might be tumorigenic and harmful to patients, they should be isolated before transplantation. We previously developed a technique for labeling DA neurons with GFP driven by the tyrosine

* Corresponding author. at Department of Physiology, Keio University School of Medicine, 35 Shinanomachi, Shinjuku-ku, Tokyo 160-8582, Japan. Tel.: +81-3-5363-3747; fax: +81-3-3357-5445.
E-mail address: hidokano@sc.itc.keio.ac.jp (H. Okano).

0304-3940/03/$ - see front matter © 2004 Elsevier Ireland Ltd. All rights reserved.
doi:10.1016/j.neulet.2004.03.074

hydroxylase (TH) gene promoter and then isolating the cells by fluorescence-activated cell sorting (FACS) [18], and in the present study, we applied it to isolation of ES-cell-derived DA neurons.

The *EB3* ES cells [15] were co-transfected with the p*TH-GFP* plasmid [18] and pMC1-neo plasmid (Stratagene) containing antibiotic resistant gene to obtain the stable transformant line *TH13D2*. They were maintained as described previously [6] in medium containing Geneticin. For differentiation, 5×10^5 *TH13D2* cells were dissociated to prepare a single-cell suspension and plated on confluent PA6 cells growing in a T-25 flask to induce neural differentiation as described previously [6]. To determine the dopamine levels in the conditioned medium, 1.3×10^5 ES cells were differentiated as above in 24-well plates for 12 days and incubated at 37 °C for 15 min in 500 μl of Hanks' balanced salt solution (HBSS) with 56 mM KCl. The conditioned medium was stabilized with 0.4 M perchloric acid and 5 mM EDTA and maintained at −80 °C until used for reverse-phase-HPLC analysis. FACS sorting of GFP^+ cells and transplantation into a rat model of Parkinson's disease were performed essentially as described previously [18]. All experimental protocols applied to animals were approved by the Animal Ethics Committee of Keio University. Female Sprague–Dawley rats (8 weeks old, weighing 180–220 g) were supplied by CLEA, Japan. Administration of 6-hydroxydopamine (6-OHDA) (2 μg/ml, Sigma) and rotational behavior due to the unilateral lesion were assessed essentially as described previously [19]. 6-OHDA was injected at the speed of 1 μl/min in the right substantia nigra (4 μl, AP −4.8 mm, ML +1.8 mm, DV −7.5 mm from bregma) and the right median forebrain bundle (4 μl, AP −4.5 mm, ML +1.6 mm, DV −7.8 mm from bregma) of adult female rats. Four weeks later, the efficacy of lesioning was assessed in all rats by testing them for ipsilateral rotational behavior and recording it on a video tape for 90 min after injection of methamphetamine (2.5 mg/kg, i.p.). The rats rotated more than 500/h were used for transplantation. FACS-sorted cells (1×10^4 cells/2 μl of differentiation medium [6], $n = 8$) or vehicle medium (2 μl, $n = 8$) were placed at the two sites in the striatum ipsilateral to the lesion (AP +1.0 mm, ML +3.0 mm, DV −5.0 mm; AP ± 0 mm, ML +3.0 mm, DV −5.0 mm) at the speed of 1 μl/min. There was no significant difference in rotation scores between the two groups (910 ± 127.6 vs. 813 ± 41.4, $P > 0.05$) before transplantation. All transplant recipients and vehicle control group were given cyclosporine A (10 mg/kg p.o., Novartis Pharma) daily. After another 4 weeks, the efficacy of transplantation was assessed in all rats by testing them for rotational behavior and recording it on a video tape after injection of methamphetamine (2.5 mg/kg, i.p.). Brain sections (50 μm) were cut on a Leica Vibratome VT1000 S (Leica Instruments) and after incubating with rabbit polyclonal anti-TH antibody (Chemicon AB152) for 48 h, with biotin-conjugated goat anti-rabbit IgG overnight, and then incubated with an ABC kit (Vector). For immunofluorescence staining, sections were incubated with rabbit polyclonal anti-TH antibody and monoclonal anti-GFP antibody (Molecular Probes A-11120) for 48 h, and then incubated with Alexa™ 488 goat anti-rabbit IgG antibody and Alexa™ 568 goat anti-mouse IgG antibody (Jackson Immuno Research) overnight for signal detection. Finally, the sections were stained with Hoechst 33342 (2 μg/ml, Sigma) to label all the nuclei. Immunohistochemical images were examined with a Zeiss-AxioCam microscope system.

To monitor induction of DA neurons by green fluorescence in vitro, we differentiated *TH13D2* cells into DA neurons by co-culture with the PA6 cells that possesses stromal-cell derived inducing activity (SDIA) [6]. Undifferentiated *TH13D2* cells do not express either TH or GFP (data not shown). During co-culture, GFP expression was detected in 36 ± 3.8% of the cells in the dishes at 4 days in vitro (DIV) ($n = 5$) and the percentage of GFP^+ cells gradually increased to 44 ± 4.1% by 12 DIV ($n = 5$) (Fig. 1A). TH expression was detected as early as 4 DIV in 3% of cells. The percentage of TH-immunoreactive cells increased to 32 ± 4.3% by 12 DIV ($n = 5$). At the end of co-culture, the cultures contained process-bearing putative DA neurons that expressed both GFP and TH, and round cells that expressed GFP but not TH (Fig. 1B). While the percentage of GFP^+ cells keep constant during co-culture, TH^+ cells increase rapidly, suggesting that the GFP^+ TH^- cells may represent precursors of TH^+ DA neurons. Consistently, the similar GFP^+ TH^- putative precursors have been found in the ventricular zone adjacent to DA neurons in the ventral mesencephalon of *TH-GFP*transgenic mouse embryos [11]. The 9-kb promoter of the rat TH gene we used in this study seems to possess *cis*-regulatory elements for transcriptional control that are sufficient for initial activation of the gene but not for the later phases. Consequently, expression of GFP in the *TH-GFP* transgenic mouse embryos started in developing midbrain DA neurons around E11–E12 and was then remarkably down-regulated during later embryonic stages [11]. Consistent with this, some of the TH-positive cells displaying the morphology of mature neurons did not express detectable GFP under our culture conditions (Fig. 1B). To confirm that these TH-positive cells were mature DA neurons, we determined secreted dopamine levels in the culture supernatant by HPLC (Fig. 1E). The total amount of dopamine production was 678 ± 79.8 pg/well per hour, and no dopamine-β-hydroxylase was detected by immunocytochemistry (data not shown). These results suggest that live DA neurons and their precursors generated from ES cells can be labeled with the *TH-GFP*reporter gene.

We previously established a method of isolating DA neurons from brain tissue of transgenic mice by FACS labeled with TH-GFP [18], and in this study we applied the same strategy to differentiated ES cells. *TH13D2* ES cells at 12 DIV after neural induction by the SDIA method were enzymatically dissociated and then analyzed for GFP fluorescence by flow cytometry (Fig. 2A,B). Dead cells

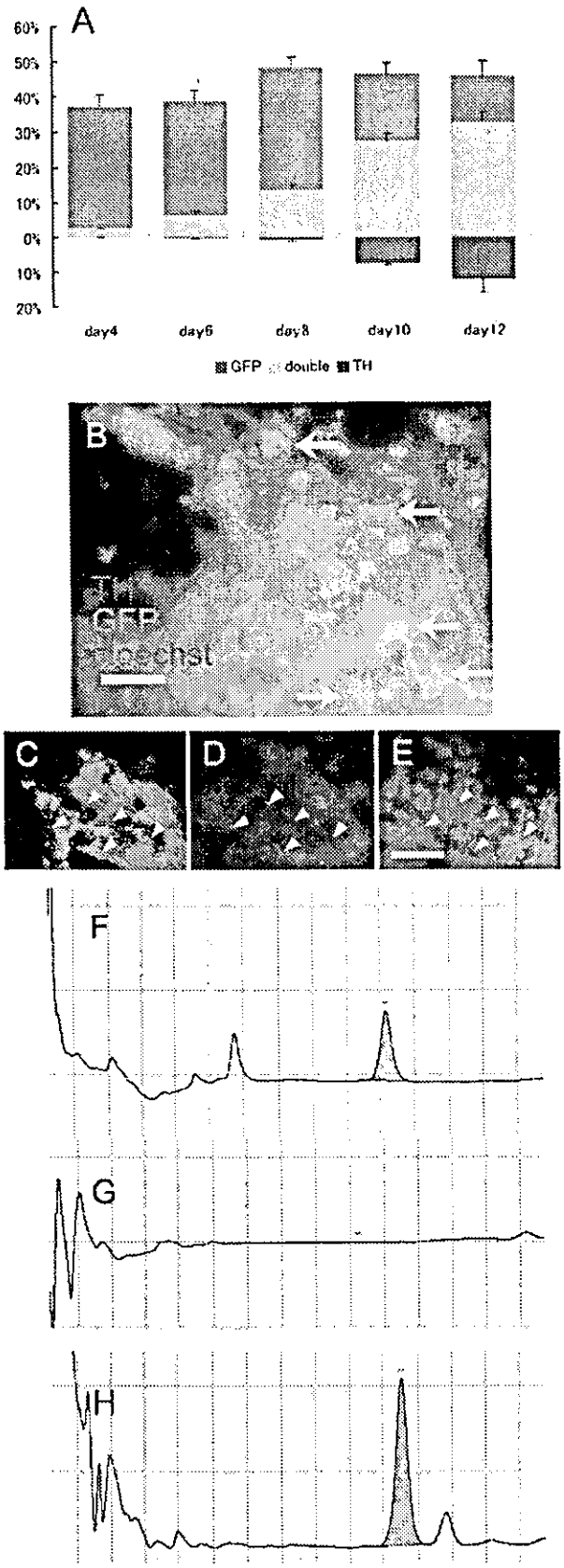

were excluded by gating on forward and side scatter as well as by elimination of propidium-iodide (PI)-positive events. To obtain a very pure population of GFP^+ DA neurons, cells were considered positive only if their fluorescence was brighter than that of the control cells. According to this criterion, only 2.66 ± 0.87% of the live cells were isolated as GFP^+ cells ($n = 5$); 89.2 ± 3.7% of GFP^+ cells were identified in the PI-positive cell population and 84.1 ± 5.3% of GFP^+ cells were identified alive ($n = 5$). These results suggest that GFP^+ cells are preferentially killed, probably because they are process-bearing neurons and can be damaged by enzymatic and physical dissociation. The sorted GFP^+ cells were examined under a fluorescence microscope. Virtually all of the cells showed GFP fluorescence (Fig. 2C), confirming that a pure population of GFP^+ cells had been obtained. The cells were then fixed and stained for TH, and 98.2 ± 2.1% of the sorted GFP^+ cells were TH^+ ($n = 5$) (Fig. 2E). By contrast, only 2.8 ± 0.79% of all sorted whole live cells were GFP^+ ($n = 5$) (Fig. 2D), and 2.7 ± 1.05% were TH/GFP double-positive ($n = 5$). Thus, sorting based on TH-GFP fluorescence yielded a highly enriched population of DA neurons.

To investigate the function of the sorted GFP^+ cells in vivo, we transplanted them into the brain of a rat model of Parkinson's disease [1]. All of the animals with unilateral 6-OHDA lesions displayed a robust rotation response to methamphetamine before transplantation without a significant difference between the transplantation group and the vehicle control group ($P > 0.05$ unpaired two-tailed Student's t-test). A total of 20,000 sorted GFP^+ cells were transplanted in the lesioned striatum of each rat in the transplantation group. Four weeks after transplantation, a significant reduction in rotational asymmetry was observed in all of the rats transplanted with GFP^+ cells, but no significant improvement was detected in the lesion control animals (pre-transplant 813 ± 41.4 vs. post-transplant 914 ± 242.2, $P > 0.05$, $n = 8$). The rotation scores of the grafted animals ($n = 8$) were reduced by an average of 15.6 ± 7.3% ($P < 0.05$) compared with the pre-transplantation scores, indicating that the grafted cells were functional in vivo.

Fig. 1. Differentiation of TH-GFP transgenic ES cells in vitro. Changes in ratio of GFP-positive (green) and TH-positive (red) cells during differentiation. TH and GFP double positive cells (yellow) increased during induction. Cells in culture (day 12) were stained with antibodies against TH (red), GFP (green), and Hoechst 33342 (blue). The photograph is a merged image of anti-GFP-stained (green), anti-TH-stained (red), and Hoechst 33342-stained (blue) cells. Some cells have neuronal appearance (arrow). Scale bar = 160 μm. (C–E) High power magnification images of the cells of neuronal morphology indicated by arrow in (B) labeled with anti-GFP antibody (C), anti-TH antibody (D) and Hoechst (E). Axon-like process is marked by arrowheads. Scale bar = 160 μm. (F,G) HPLC detection of dopamine secreted in the DA standard with medium (F), medium control (G), and conditioned medium of DA neurons stimulated with KCl (H).

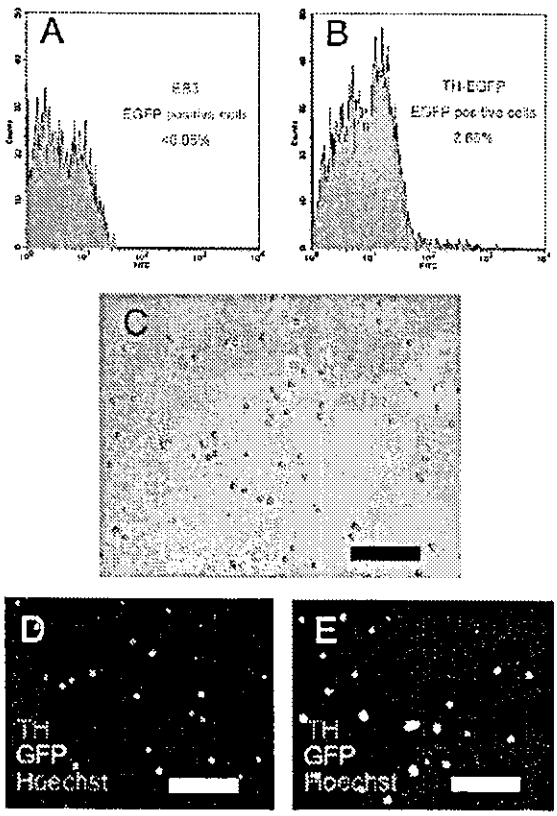

Fig. 2. Isolation of GFP-positive cells by FACS. After induction (12 DIV) cells from the control ES cell culture (A) and TH13D2 cell culture (B) were analyzed with a FACS. Virtually all the sorted cells show GFP fluorescence (C). Scale bar = 200 μm. Unsorted (D) and sorted GFP$^+$ (E) cells were directly attached to slides and fixed and stained with an antibody against TH (red), and GFP (green), and Hoechst 33342 (blue). The photographs are merged images of anti-GFP-stained (green), anti-TH-stained (red), and Hoechst 33342-stained (blue) cells. Scale bar = 200 μm.

Brain sections were stained with anti-TH antibody and anti-GFP antibody to identify grafted cells (Fig. 3B,C). The 6-OHDA lesions caused a virtually complete loss of TH$^+$ DA neurons in the substantia nigra and concomitant depletion of TH-immunoreactive fibers in the lesioned striatum (data not shown). Grafts that contained GFP$^+$ and TH$^+$ double-positive cells were found in the striatum of the rats transplanted with the GFP$^+$ cells (Fig. 3B,C), and some of the TH$^+$ cells in the grafts displayed morphological features suggestive of mature neurons and had extended TH$^+$ fibers into the host striatum (Fig. 3D). Taken together, these results show that the isolated GFP$^+$ cells differentiated into mature DA neurons in the host striatum and were functional and improved amphetamine-induced rotational asymmetry in a rat model of Parkinson's disease. ES-cell derived sorted GFP-positive cells, however, were less effective (77.3% vs. 15.6%) in achieving rotational recovery than transplantation of sorted GFP-positive cells from the ventral mesencephalon of TH-GFP transgenic mouse in our previous study [18]. Thus, the protocol for preparation of DA neurons from ES cells needs to be modified to increase

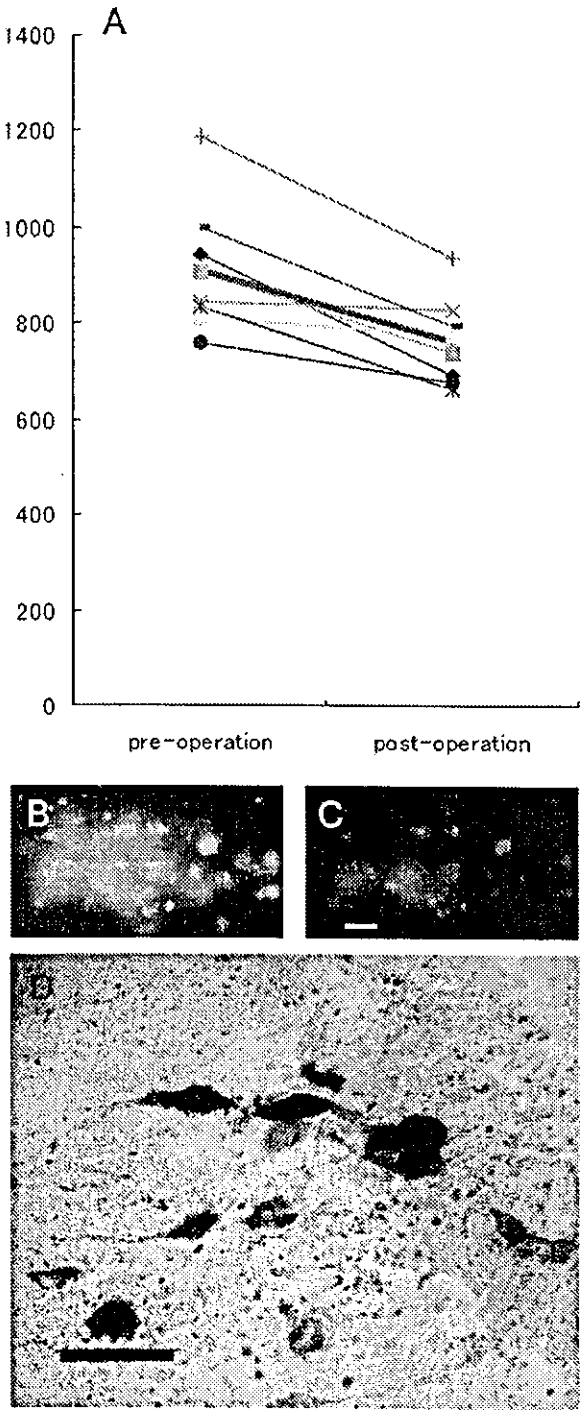

Fig. 3. Transplanted EGFP$^+$ cells caused functional recovery in a rat model of Parkinson's disease. (A) Net ipsilateral amphetamine-induced rotation asymmetry over the 90-min test session. All of the animals with grafts showed steady improvement compared with pre-graft rotation. Average rotations are represented by the thick red line. (B,C) The transplantation site. Grafted cells expressing both GFP (B) and TH (C) can be seen in the striatum. Scale bar = 80 μm. (D) High power magnification view of TH$^+$ neurons in the graft. The grafted TH-positive cells display the morphology of mature DA neurons. Scale bar = 80 μm.

the efficiency of recovery. Modification for obtaining higher amount of mature neurons in vitro such as administration of growth factors would be needed, or preparation conditions that mimic the differentiation of ventral mesencephalon. The number of surviving cells was much lower when dissociated cells were transplanted than when colonies were transplanted, indicating that colonies are more efficient for implanting TH-positive cells in vivo than cell suspension conditions [12]. Administration of neurotrophic factors should improve the survival of transplanted DA neurons [14].

To compare the tumorigenicity of the donor cells, we co-cultured the *CAG-GFP* ES cells that express GFP constitutively and *TH13D2* cells with PA6 cells for only 4 days, and transplanted sorted GFP^+ cells into the striatum. Four weeks later, we found tumor formation only in the brains that received the CAG-GFP-sorted mixed cell population (data not shown). These results suggest that transplantation of unsorted ES-derived cells may cause formation of a tumor in the brain, which may be prevented by use of FACS-isolated DA neurons.

In conclusion, we have demonstrated that ES-cell-derived functional DA neurons can be labeled with the TH-GFP reporter gene and isolated by FACS. This novel system should be useful for cellular and molecular studies of DA neurons and for clinical applications in the treatment of Parkinson's disease, and, in particular, it may significantly reduce the risk of tumor formation by ES-derived neural cells after transplantation.

Acknowledgements

We thank T. Nakano for the PA6 cells, H. Niwa for the EB3 ES cells and H.J. Okano for valuable discussion. This work was supported by a grant from the Ministry of Education, Science, Sports, Culture and Technology, a grant from CREST of the Japan Science and Technology Agency, and a grant-in-aid from the 21st Century COE Program of the Ministry of Education, Science and Culture to Keio University.

References

[1] M.F. Beal, Experimental models of Parkinson's disease, Nat. Review Neurosci. 2 (2001) 325–332.
[2] A. Björklund, S.B. Dunnett, P. Brundin, A.J. Stoessl, C.R. Freed, R.E. Breeze, M. Levivier, M. Peschanski, L. Studer, R. Barker, Neural transplantation for the treatment of Parkinson's disease, Lancet Neurol. 2 (2003) 437–445.
[3] L.M. Bjorklund, O. Isacson, Regulation of dopamine cell type and transmitter function in fetal and stem cell transplantation for Parkinson's disease, Prog. Brain Res. 138 (2002) 411–420.
[4] O. Isacson, L.M. Bjorklund, J.M. Schumacher, Toward full restoration of synaptic and terminal function of the dopaminergic system in Parkinson's disease by stem cells, Ann. Neurol. 53 (2003) S135–S148.
[5] O. Isacson, L. Costantini, J.M. Schumacher, F. Cicchetti, S. Chung, K.S. Kim, Cell implantation therapies for Parkinson's disease using neural stem, transgenic or xenogeneic donor cells, Parkinson Relat. Disord. 7 (2001) 205–212.
[6] H. Kawasaki, K. Mizuseki, S. Nishikawa, S. Kaneko, Y. Kuwana,, S. Nakanishi, S.I. Nishikawa, Y. Sasai, Induction of midbrain dopaminergic neurons from ES cells by stromal cell-derived inducing activity, Neuron 28 (2000) 31–40.
[7] J.H. Kim, J.M. Auerbach, J.A. Rodriguez-Gomez, I. Velasco, D. Gavin, N. Lumelsky, S.H. Lee, J. Nguyen, R. Sanchez-Pernaute, K. Bankiewicz, R. McKay, Dopamine neurons derived from embryonic stem cells function in an animal model of Parkinson's disease, Nature 418 (2002) 50–56.
[8] J.Y. Kim, H.C. Koh, J.Y. Lee, M.Y. Chang, Y.C. Kim, H.Y. Chung, H. Son, Y.S. Lee, L. Studer, R. McKay, S.H. Lee,, Dopaminergic neuronal differentiation from rat embryonic neural precursors by Nurr1 overexpression, J. Neurochem. 85 (2003) 1443–1454.
[9] S.H. Lee, N. Lumelsky, L. Studer, J.M. Auerbach, D. McKay, Efficient generation of midbrain and hindbrain neurons from mouse embryonic stem cells, Nat. Biotech. 18 (2000) 675–679.
[10] O. Lindvall, P. Brundin, H. Widner, S. Rehncrona, B. Gustavii, R. Frackowiak, L.S. Leenders, G. Sawle, J.C. Rothwell, C.D. Marsden, A. Bjorklund, Grafts of fetal dopamine neurons survive and improve motor function in Parkinson's disease, Science 247 (1990) 574–577.
[11] N. Matsushita, H. Okada, Y. Yasoshima, K. Takahashi, K. Kiuchi, K. Kobayashi, Dynamics of tyrosine hydroxylase promoter activity during midbrain dopaminergic neuron development, J. Neurochem. 82 (2002) 295–304.
[12] A. Morizane, J. Takahashi, Y. Takagi, Y. Sasai, N. Hashimoto, Optimal conditions for in vivo induction of dopaminergic neurons from embryonic stem cells through stromal cell-derived inducing activity, J. Neurosci. Res. 69 (2002) 934–939.
[13] T. Nagatsu, T. Yamaguchi, M.K. Rahman, J. Trocewicz, K. Oka, Y. Hirata, I. Nagatsu, H. Narabayashi, T. Kondo, R. Iizuka, Catecholamine-related enzymes and biopterin cofactor in Parkinson's diseases, in: R.G. Hasseler, J.F. Christ (Eds.), Advances in Neurology, 40, Raven, New York, 1984, pp. 467–473.
[14] K. Nakajima, H. Hida, Y. Shimano, I. Fujimoto, T. Hashitani, M. Kumazaki, T. Sakurai, H. Nishino, GDNF is a major component of trophic activity in DA-depleted striatum for survival and neurite extension of DAergic neurons, Brain Res. 916 (2001) 76–84.
[15] H. Niwa, J. Miyazaki, A.G. Smith, Quantitative expression of Oct-3/4 defines differentiation, dedifferentiation or self-renewal of ES cells, Nat. Genet. 24 (2000) 372–376.
[16] P. Piccini, D.J. Brooks, A. Björklund, R.N. Gunn, P.M. Grasby, O. Rimoldi, P. Brundin, P. Hagell, S. Rehncrona, H. Widner, O. Lindvall, Dopamine release from nigral transplants visualized in vivo in a Parkinson's patient, Nat. Neurosci. 2 (1999) 1137–1140.
[17] S.S. Riaz, E. Jauniaux, G.M. Stern, H.F. Bradford, The controlled conversion of human neural progenitor cells derived from foetal ventral mesencephalon into dopaminergic neurons in vitro, Dev. Brain Res. 136 (2002) 27–34.
[18] K. Sawamoto, N. Nakao, K. Kobayashi, N. Matsushita, H. Takahashi, K. Kakishita, A. Yamamoto, T. Yoshizaki, T. Terashima, F. Murakami, T. Itakura, H. Okano, Visualization, direct isolation, and transplantation of midbrain dopaminergic neurons, Proc. Natl. Acad. Sci. USA 98 (2001) 6423–6428.
[19] U. Ungerstedt, W. Arbuthnott, Quantitative recording of rotational behavior in rats after 6-hydroxy-dopamine lesions of the nigrostriatal dopamine system, Brain Res. 24 (1970) 485–493.
[20] G.K. Wenning, P. Odin, P. Morrish, S. Rehncrona, H. Widner, P. Brundin, J.C. Rothwell, R. Brown, B. Gustavii, P. Hagell, M. Jahanshahi, G. Sawle, A. Bjorklund, D.J. Brooks, C.D. Marsden, N.P. Quinn, O. Lindvall, Short- and long-term survival and function of unilateral intrastriatal dopaminergic grafts in Parkinson's disease, Ann. Neurol. 42 (1997) 95–107.

Skeletal Radiol (2004) 33:524–530
DOI 10.1007/s00256-004-0815-5

ARTICLE

Hong Zhang
Kyosan Yoshikawa
Katsumi Tamura
Kenji Sagou
Mei Tian
Tetsuya Suhara
Susumu Kandatsu
Kazutoshi Suzuki
Shuji Tanada
Hirohiko Tsujii

Carbon-11-methionine positron emission tomography imaging of chordoma

Received: 27 September 2003
Revised: 12 May 2004
Accepted: 13 May 2004
Published online: 28 July 2004

This study was part of the 10-Year Strategy for Cancer Control of the Japanese Government and was supported by the Ministry of Education, Science and Technology of Japan Government

H. Zhang · M. Tian · T. Suhara · K. Suzuki · S. Tanada
Department of Medical Imaging,
National Institute of Radiological Sciences,
Chiba, Japan

H. Zhang
Department of Medical Imaging,
Research Center Hospital
for Charged Particle Therapy,
National Institute of Radiological Sciences,
4-9-1, Anagawa, Inage-ku, 263-8555 Chiba,
Japan

K. Yoshikawa (✉) · K. Tamura · K. Sagou · S. Kandatsu
Clinical Diagnosis Section,
National Institute of Radiological Sciences,
Chiba, Japan
e-mail: kyo_yosi@nirs.go.jp
Tel.: +81-43-2512111
Fax: +81-43-2063370

H. Tsujii
Research Center
for Charged Particle Therapy,
National Institute of Radiological Sciences,
Chiba, Japan

Abstract *Objective:* Chordoma is a rare malignant bone tumor that arises from notochord remnants. This is the first trial to investigate the utility of ^{11}C-methionine (MET) positron emission tomography (PET) in the imaging of chordoma before and after carbon-ion radiotherapy (CIRT). *Design and patients:* Fifteen patients with chordoma were investigated with MET-PET before and after CIRT and the findings analyzed visually and quantitatively. Tumor MET uptake was evaluated by tumor-to-nontumor ratio (T/N ratio). *Results:* In 12 (80%) patients chordoma was clearly visible in the baseline MET-PET study with a mean T/N ratio of 3.3±1.7. The MET uptake decreased significantly to 2.3±1.4 after CIRT ($P<0.05$). A significant reduction in tumor MET uptake of 24% was observed after CIRT. Fourteen (93%) patients showed no local recurrence after CIRT with a median follow-up time of 20 months. *Conclusion:* This study has demonstrated that MET-PET is feasible for imaging of chordoma. MET-PET could provide important tumor metabolic information for the therapeutic monitoring of chordoma after CIRT.

Keywords Chordoma · ^{11}C-methionine · PET · Carbon ion radiotherapy · Diagnosis

Introduction

Chordoma is a rare malignant neoplasm representing less than 3% of all primary bone tumors. It usually has a benign histological appearance and a slow growth rate. It has little metastatic potential, but considerable local destructiveness [1]. Since almost all the lesions arise in the spine or skull base with about 50% of chordomas of sacrococcygeal origin [2], a small difference in the tumor extent can have profound clinical consequences. Efforts to increase local control have included aggressive surgery, radiation therapy or combined approaches, but locally-free survival rates remain relatively low and have not exceeded 30% at 5 years [3]. As total surgical resection is often not feasible, other management strategies must frequently be considered [4, 5, 6]. Traditionally, this tumor has been considered to be "radioresistant" to standard-dose radiation therapy [7]. To improve the radiobiological effect, fractionated irradiation with charged particles has been introduced in our institute and reported with encouraging results [8, 9, 10]. Since chordoma is slow-growing and most of the treated patients show no significant decrease in tumor volume, the early response of chordoma after charged particle therapy may be difficult to evaluate by anatomical imaging modalities alone. Furthermore, it is crucial that the active and aggressive regions of tumor are defined accurately both before charged particle therapy and for follow-up of treatment, to form the basis for further accurate treatment planning and delivery of radiation therapy.

It has been shown that ^{18}F-fluorodeoxyglucose (FDG) positron emission tomography (PET) is valuable for the detection, staging, grading and monitoring of therapy of various tumors [11, 12], although the usefulness of FDG-PET in the early evaluation of chemotherapy or radiotherapy is still a matter of debate, since increased FDG uptake can occur in macrophages, neutrophils, fibroblasts and granulation tissue immediately after therapy [13, 14, 15]. However, as an essential amino acid, L-methionine plays a central role in the altered metabolism of cancer cells [16]. L-[methyl-^{11}C]-methionine (MET) uptake correlates with cell proliferation in cell culture, Ki-67 expression and proliferating cell nuclear antigen expression, indicating its role as a marker for active tumour proliferation [17]. Autoradiographic findings reported by Kubota et al. [18] demonstrate that the level of increased MET uptake correlates with the number of tumor cells, whereas no significant MET uptake occurs in chronic inflammatory or radiogenic lesions. Preclinical studies validating the possible use of MET in the evaluation of chemo- or radiotherapy generally show that MET uptake is reduced rapidly—more rapidly than that of FDG [19, 20, 21]—and that MET uptake correlates better than FDG with tumor proliferative activity in squamous cell head and neck cancer cell lines [22]. In addition, increased uptake of MET as measured by PET has been suggested to reflect increased transport, transmethylation rate and protein synthesis of malignant tissue [22, 23, 24, 25], and is less influenced by radiation-induced inflammatory reaction after radiotherapy compared with FDG [21]. We therefore chose MET-PET to evaluate the early response of chordoma after charged particle carbon ion radiotherapy (CIRT). Our hypothesis was that chordoma shows high amino acid metabolism that decreases within a few days after CIRT, thus providing the potential for imaging and monitoring of chordoma treated by CIRT. To our knowledge, no other studies have reported the imaging of chordoma with MET-PET. In this paper, we report our initial experience in the imaging of chordoma with MET-PET before and after CIRT.

Patients and methods

Patients

This study comprised a total of 30 MET-PET scans carried out on15 chordoma patients (11 men, 4 women) with a mean age of 66 years (SD ±13). Table 1 presents the patient characteristics and the results of the MET-PET study. All patients had a complete history and physical examination, including radiography, computed tomography (CT) or magnetic resonance imaging (MRI), prior to MET-PET. Based on the clinical findings, tumor was considered to be present in all patients without distant metastases. Tumors were grossly measured, but size did not exceed 15 cm. Tumors were judged to be unresectable by the referring surgeon, or the patients were medically inoperable or declined surgery. Histological diagnosis was confirmed by tumor biopsy and histological grading was performed according to the World Health Organization (WHO) classification [26]. After CIRT, invasive biopsy was not performed in order to get an uncontaminated follow-up for the therapeutic response to carbon ion radiotherapy. Patients who had undergone chemotherapy within 4 weeks before carbon ion radiotherapy or those who had prior radiation therapy at the same site were excluded from the study. All patients signed the informed consent form approved by our institutional review board.

PET imaging

^{11}C-MET was prepared by a method modified from the synthesis of Langstrom et al. [27]. Whole-body scanners (ECAT EXACT HR+ and ECAT EXACT 47; Siemens CTI, Knoxville, Tenn.) were used, providing an axial field of view of 15.5 and 16.2 cm, resulting in 63 and 47 transverse slices with a thickness of 2.5 and 3.4 mm, respectively. The spatial resolution of the reconstructed images is 4.2–6.0 mm at full-width half maximum. Transmission scans were performed with germanium-68 rod sources. Emission data corrected for random events, dead time and attenuation were reconstructed by filtered backprojection using a ramp filter with a cutoff frequency of 0.4, followed by the decay correction.

Before initiation of CIRT, a baseline MET-PET was performed and MET-PET was repeated within 1 month after completion of CIRT. Patients fasted for at least 4 h before PET imaging. Before MET injection, all patients underwent a transmission scan for one (ECAT EXACT HR+) or two bed positions (ECAT EXACT 47) including the lesion site, each bed position for 20 and 10 min for ECAT EXACT HR+ and ECAT EXACT 47, respectively. Static emission data for the same positions were obtained from 23 min after the intravenous administration of approximately 740 MBq of

Table 1 Patient characteristics and PET results (*R* recurrence, *P* primary tumor, *M* metastases, *n* no, *y* yes)

Patient no.	Gender	Age (years)	Presentation	Location	Size (cm)	Grade	Radiation dose (GyE)	T/N ratio before	T/N ratio after	%T/N ratio	Local recurrence
1	M	70	R	Ilium	13	–	52.8	4.9	3.7	0.24	n
2	M	71	R	Pelvic wall	12	–	70.4	7.1	6.4	0.10	n
3	F	59	P	Sacrum	12	Gx	73.6	3.5	3.0	0.13	n
4	M	69	P	Sacrum	15	Gx	73.6	1.0	1.0	0.01	y (12 months)
5	M	71	P	Sacrum	10	Gx	73.6	3.2	2.6	0.18	n
6	M	85	P	Sacrum	13.5	Gx	73.6	3.2	2.6	0.18	n
7	F	80	R	Thoracic spine	7	–	70.4	3.8	1.2	0.67	n
8	M	65	P	Sacrum	9	Gx	73.6	0.8	0.9	–0.12	n
9	F	41	P	Sacrum	10	Gx	70.4	1.4	1.0	0.29	n
10	M	41	R	Sacrum	7.8	–	70.4	3.0	2.3	0.25	n
11	M	65	P	Sacrum	10	Gx	70.4	4.4	2.2	0.50	n
12	M	57	P	Sacrum	8	Gx	70.4	5.4	1.8	0.66	n
13	F	64	P	Sacrum	10	Gx	70.4	3.6	1.7	0.52	n
14	M	66	P	Sacrum	7	Gx	70.4	1.9	1.8	0.03	n
15	M	85	M	Thigh	14	–	70.4	2.9	2.8	0.02	n

MET [28]. Because of the difference in sensitivity of the PET scanners, static emission scans were performed for 30 min in ECAT EXACT HR+ and 15 min in ECAT EXACT 47 for each bed position, respectively.

Image analysis

Tomographic images displayed as coronal, sagittal and transaxial slices were viewed on a workstation. Two experienced nuclear medicine physicians (H.Z. and K.Y.) evaluated the PET images for the presence of regional metabolic activity. For quantitative evaluation, regions of interest (ROI) with a diameter of 1 cm were manually drawn over these heterogeneous tumors in the transaxial slice with maximum MET uptake on the baseline scan to reflect the most metabolically active area of the tumor. The most metabolically active areas are thought to reflect tumor regions with more aggressive tumor. The inherent assumption was made that the overall behavior of the tumor is predicted by the activity of the most aggressive regions. The ROIs for the background radioactivity measurement were drawn on the homologous contralateral or surrounding normal tissue. Tumor-to-nontumor ratio (T/N ratio) was calculated using the following formula: T/N ratio = mean counts per pixel of tumor ROI/mean counts per pixel of normal tissue ROI. The percentage reduction in the T/N ratio (%T/N ratio) after CIRT was calculated as:

$$\%\text{T/N ratio} = 1 - \frac{\text{T/N ratio after CIRT}}{\text{T/N ratio before CIRT}}.$$

Statistics

Data were expressed as mean±SD. Student's *t*-test was used for the statistical analysis. A difference with $P<0.05$ was considered significant.

Results

Table 1 shows the characteristics of the patients and the results of the MET-PET studies. Eleven tumors were in Gx and four were recurrent tumors. No patient had received chemotherapy over the 4 weeks prior to the initiation of CIRT. Variable baseline MET uptakes were observed in tumors, the T/N ratio ranging from 0.8 to 7.1 with a mean value of 3.3±1.7. The mean T/N ratio was 2.8±1.4 (range 0.8–5.4) for primary tumors and 4.7±1.8 (range 3.0–7.1) for recurrent lesions. It was found that MET uptake in recurrent lesions was significantly higher than that of primary tumors ($P<0.03$). All four recurrent lesions were identified on MET-PET imaging, while eight of 11 (73%) primary tumors could be visualized and three (27%) primary lesions were negative. Overall, tumor area was clearly visible in the baseline PET study in 12 of 15 (80%) patients. Typical examples are shown in Figs. 1 and 2. It should be noted that inhomogeneous MET uptake could be observed in some cases, which reflected the variety of the components, such as fluid and gelatinous mucoid substance, associated with recent and old hemorrhages, and necrotic areas within chordoma, and as well as calcification and sequestered bone fragments. Delineation of one tumor (patient 9) was difficult because of the low MET uptake. However, the tumor could still be delineated from the image when the anatomical location of the tumor was known by the authors before image interpretation.

All the patients had a second PET study within 1 month after CIRT. Tumor MET accumulation visibly decreased and the mean T/N ratio decreased to 2.3±1.4 (range 0.9–6.4). The difference between the two mean T/N ratios was significant ($P<0.05$) (Fig. 3). The reductions in MET uptake by the patients after CIRT is shown in Fig. 4. A mean MET uptake reduction of 24%±24% was observed after CIRT. Eleven of 12 patients with positive initial MET studies had a reduction in MET uptake with a mean value of 33.8%. All 11 patients had an MET uptake reduction of more than 10%, whereas one patient had over a 10% increase and three patients showed no change. Of the 11 patients, seven (64%) showed a significant reduction of more than 20%, and four (36%) showed a reduction of more than 30%. The patients were followed up for up to

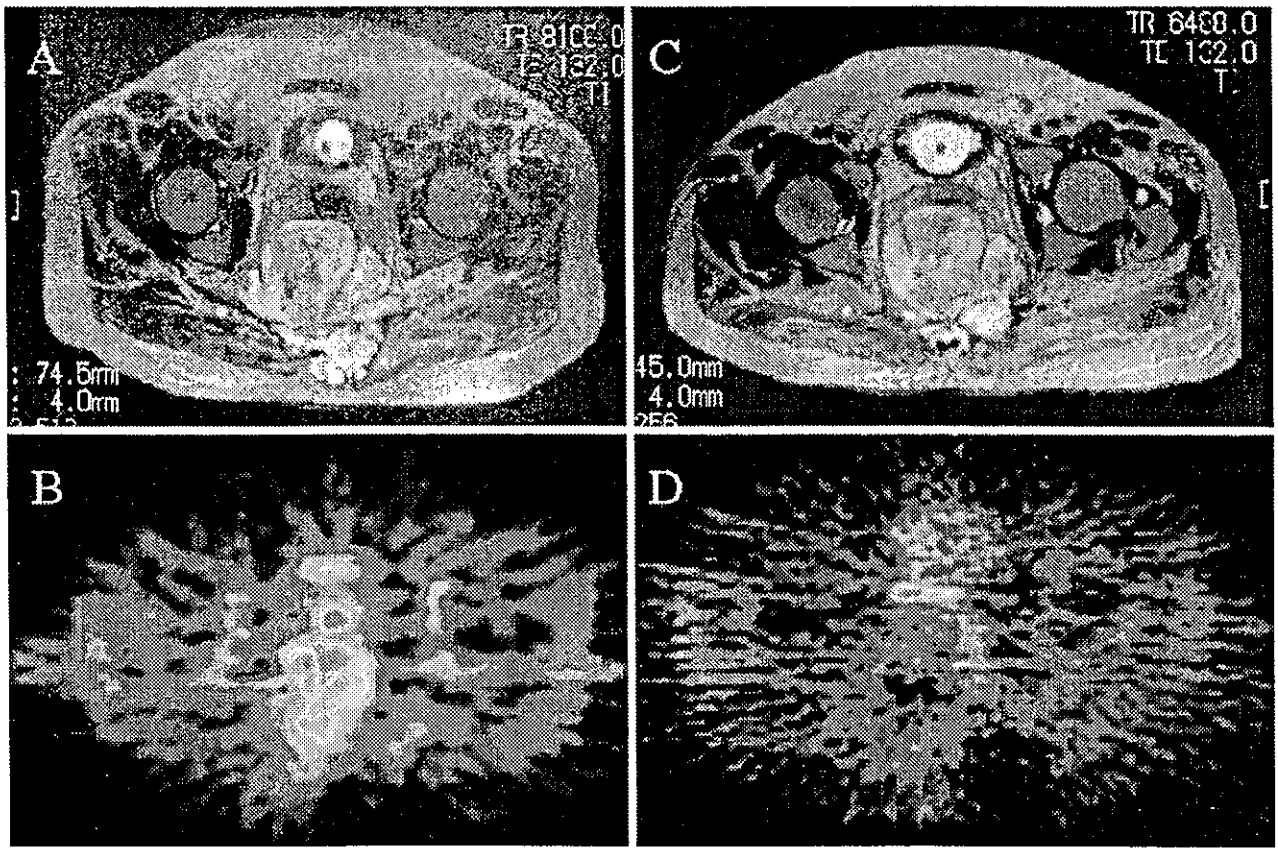

Fig. 1A–D Case 11. A 65-year-old man who received 70.4 GyE to chordoma in the sacrum. **A** MR image of the pelvis showed a large heterogeneous mass in the sacrum. **B** Baseline MET uptake demonstrated an inhomogeneous mass in the same region. **C** MR image still revealed a large mass after CIRT. **D** Tumor MET uptake decreased significantly after CIRT

5 years for therapeutic evaluation. Only one patient was diagnosed as having a local recurrence after CIRT. Time to local recurrence was 12 months (patient 4). Because of the very small population, the correlation between local recurrence and MET uptake could not be analyzed.

Discussion

CIRT has shown promising local control rates in excess of 73% at 3 years, contrasting with the approximately 35% control rate reported with conventional radiation [10, 29, 30]. As this is a new treatment technique, there is a need for accurate assessment of the early response of tumor as well as the follow-up of the patients. Current imaging methods including CT and MRI have limitations in distinguishing viable tumor from post-therapeutic changes because of changes in normal anatomy, distortion of tissue planes, and lack of distinction between tumor and post-therapeutic tissue [31, 32]. These traditional radiographic methods for assessing response to therapy are poorly suited to evaluating osseous lesions [33]. Although peritumoral edema and in some cases extraosseous soft tissue masses may be reduced around osseous tumors, traditional radiographic studies are unable to distinguish nonresponding from responding lesions [34]. In this study, invasive biopsy was not performed after CIRT in order to obtain an uncontaminated follow-up study of the therapeutic response to CIRT. Our data clearly demonstrate the feasibility of MET-PET, which yielded a sensitivity of 80% (12/15) in the visualization of all lesions and 100% (4/4) for the recurrent tumors. Patients who had recurrent tumors tended to have high baseline MET uptake, which probably reflects the tendency to malignant transformation in progressive tumors. Primary tumors showed variable uptakes in this study, and it was not possible to evaluate therapeutic assessment of chordoma when there was a negative finding on baseline MET-PET image. Chordoma has variable growth rates [4, 5], which may be due to differing metabolic activity and resulted in differing accumulation of MET in our study. Second, all the primary tumors in this study had an undifferentiated pathological grade (Gx), which might include variable malignant cells, which are different for each tumor. This

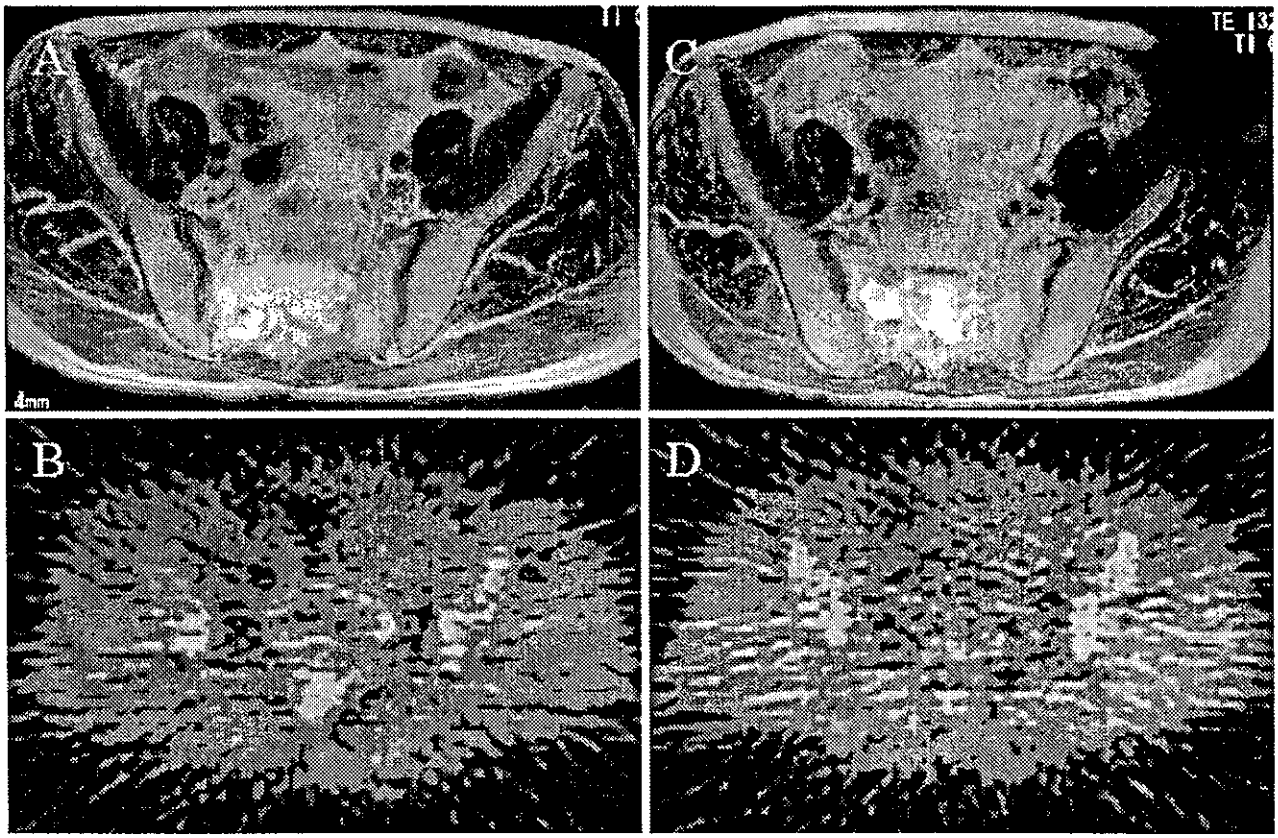

Fig. 2A–D Case 8. A 65-year-old man who received 73.6 GyE to chordoma in the sacrum. **A, C** MR images showed a large mass at the sacrum before (**A**) and after CIRT (**C**). **B, D** However, no significant MET uptake was observed on PET images either before (**B**) or after (**D**) CIRT

could be a partial explanation for the variable MET accumulations in this study. Factors such as gender, age, tumor size and pre-CIRT therapy were not found to affect MET accumulation statistically.

Tumor MET accumulation was evaluated by the T/N ratio in this study, as it has been shown that semiquantitative analysis by SUV is not as reliable as the tumor-to-liver ratio in evaluation of tumor response to fluorouracil in colorectal cancer liver metastases [35]. This is indicative of the problems of introducing extra measurement variables when trying to establish a semiquantitative method. Inadequate injection with extravasation of some of the MET at the time of intravenous administration most likely led to an underestimate of the tumor SUV. This problem did not affect the tumor-to-background ratio as injected activity is irrelevant. A further potential confounding factor for SUV calculation of MET is that a competing organ such as the liver could take up a greater proportion of the injected MET dose, leaving less for the tumor. If this is present only on the pretreatment or post-treatment scan, it may result in a misinterpretation of the tumor response.

Muhr et al. investigated the metabolic reduction of tumor in connection with the effectiveness of interferon-α (IFN-α) treatment in meningioma [36]. After IFN-α treatment, tumors were observed at biopsy to be changed into fibrous-rich tissue with fewer viable tumor cells but had not decrease in size compared with before treatment [37]. Their study suggested that in tumor treatment it is important to demonstrate decreased tumor metabolism as a sign of decreased tumor growth but not necessarily diminished tumor volume. In this study, our results demonstrated that CIRT was effective in reducing tumor metabolism. The measurements of chordoma size, including intraosseous extent on either T1-weighted or short inversion time inversion recovery (STIR) MRI, did not change significantly after CIRT and were difficult to assess in some patients. Chordomas in this study were mainly located in the sacrum, and the bladder sometimes showed a similar MET uptake compared with tumor tissue. However, due to the anatomical localization of the tumors, this did not interfere with scan interpretation.

It is known that fluid and gelatinous mucoid substance, associated with recent and old hemorrhages, and necrotic

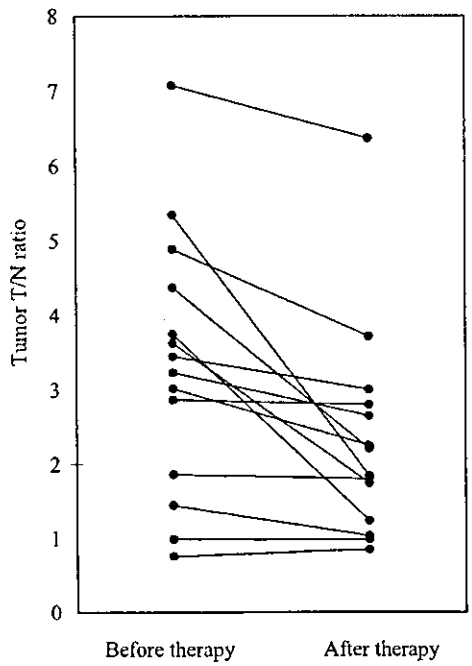

Fig. 3 Changes in MET uptake by the chordoma following CIRT. A significant reduction of MET-PET was observed ($P<0.05$)

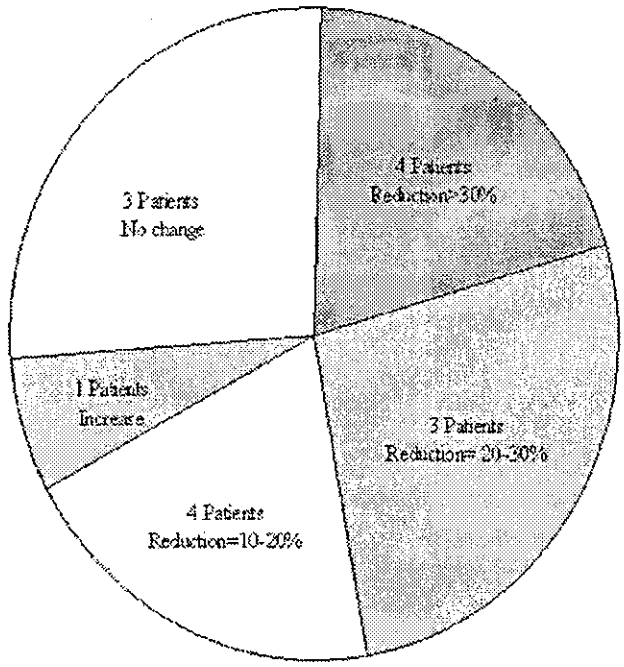

Fig. 4 The changes in MET uptake in patients after CIRT

areas are found within chordoma, and in some cases calcification and sequestered bone fragments reflect the type of tissue or matrix in the tumor. Different parts within a tumor may have different malignancy grades. In this MET-PET study it was found that MET uptake could be variable within a tumor before CIRT. After CIRT, MET-PET showed peripheral areas of higher metabolic activity and central areas of decreased or no activity, suggestive of tumor necrosis. These important biological characteristics are immediately apparent on MET-PET imaging and available for clinical decision-making. In addition, it would be potentially advantageous to recognize the presence of residual viable tumor in both the planning of post-treatment therapy and during the follow-up phase for demonstration of progressive disease. Thus, MET-PET might provide important information about metabolic activity and might be useful in treatment planning as well as post-therapeutic assessment.

It should be noted that there were several limitations to this study. Firstly, as most of the patients had Gx chordoma, it was impossible to evaluate whether MET-PET could be used for the histological grading of chordoma. Secondly, histological confirmation of suspicious imaging abnormalities should be the gold standard for post-therapeutic assessment, but in clinical practice that is unrealistic. Invasive biopsy after CIRT was not performed in order to avoid interference in the follow-up for the therapeutic response to CIRT. Thus the MET uptake changes in the tumor could not be correlated with histological confirmation after CIRT. Nevertheless, MET-PET could be worthy of a suitable indicator for post-therapeutic assessment, since a significant reduction in MET uptake after CIRT showed a good local control of tumor over a relative long period in this study. Longer follow-up will be required to determine the true significance of MET accumulation and its relationship with prognosis.

In conclusion, this study demonstrated that MET-PET is feasible for imaging of chordoma. MET-PET could provide important tumor metabolic information for the therapeutic monitoring of chordoma after CIRT.

References

1. Baratti D, Gronchi A, Pennacchioli E, et al. Chordoma: natural history and results in 28 patients treated at a single institution. Ann Surg Oncol 2003; 10:291-296.
2. Mindell ER. Chordoma. J Bone Joint Surg Am 1981; 63:501–505.
3. Breteau N, Demasure M, Lescrainier J, Sabbattier R, Michenet P. Sacrococcygeal chordomas: potential role of high LET therapy. Recent Results Cancer Res 1998; 150:148-155.
4. Watkins L, Khudados ES, Kaleoglu M, Revesz T, Sacares P, Crockard HA. Skull base chordomas: a review of 38 patients, 1958–88. Br J Neurosurg 1993; 7:241-248.
5. Gay E, Sekhar LN, Rubinstein E, et al. Chordomas and chondrosarcomas of the cranial base: results and follow-up of 60 patients. Neurosurgery 1995; 36:887-897.
6. Al-Mefty O, Borba LA. Skull base chordomas: a management challenge. J Neurosurg 1997; 86:182-189.
7. Krayenbuhl H, Yasargil MG. Cranial chordomas. Progr Neurol Surg 1975; 6:380–434.
8. Benk V, Liebsch NJ, Munzenrider JE, Efird J, McManus P, Suit H. Base of skull and cervical spine chordomas in children treated by high-dose irradiation. Int J Radiat Oncol Biol Phys 1995; 31:577–581.
9. Castro JR, Collier JM, Petti PL, et al. Charged particle radiotherapy for lesions encircling the brain stem or spinal cord. Int J Radiat Oncol Biol Phys 1989; 17:477–484.
10. Kamada T, Tsujii H, Tsuji H, et al. Working Group for the Bone and Soft Tissue Sarcomas. Efficacy and safety of carbon ion radiotherapy in bone and soft tissue sarcomas. J Clin Oncol 2002; 20:4466–4471.
11. Gambhir SS. Molecular imaging of cancer with positron emission tomography. Natl Rev Cancer 2002; 2:683–693.
12. Zhang H, Tian M, Oriuchi N, Higuch, T, Tanada S, Endo K. Oncological diagnosis using positron coincidence gamma camera with fluorodeoxyglucose in comparison with dedicated PET. Br J Radiol 2002; 75:409–416.
13. Kubota R, Yamada S, Kubota K, Ishiwata K, Tamahashi N, Ido T. Intratumoral distribution of fluorine-18-fluorodeoxyglucose in vivo: high accumulation in macrophages and granulation tissues studied by microautoradiography. J Nucl Med 1992; 33:1972—1980.
14. Haberkorn U, Strauss LG, Dimitrakopoulou A, et al. PET studies of fluorodeoxyglucose metabolism in patients with recurrent colorectal tumors receiving radiotherapy. J Nucl Med 1991; 32:1485–1490.
15. Hautzel H, Muller-Gartne, HW. Early changes in fluorine-18-FDG uptake during radiotherapy. J Nucl Med 1997; 38:1384–1386.
16. Hoffman RM. Unbalanced transmethylation and the perturbation of the differentiated state leading to cancer. Bioessays 1990; 12:163–166.
17. Kracht LW, Friese M, Herholz K, et al. Methyl-[^{11}C]-L-methionine uptake as measured by positron emission tomography correlates to microvessel density in patients with glioma. Eur J Nucl Med Mol Imaging 2003; 30:868—873.
18. Kubota R, Kubota K, Yamada S, et al. Methionine uptake by tumor tissue: a microautoradiographic comparison with FDG. J Nucl Med 1995; 36:484–492.
19. Schaider H, Haberkorn U, Berger MR, Oberdorfer F, Morr I, van Kaick G. Application of alpha-aminoiosbutyric acid,L-methionine, thymidine and 2-fluoro-2-D-glucose to monitor effects of chemotherapy in a human colon carcinoma cell line. Eur J Nucl Med 1996; 23:55–60.
20. Higashi K, Clavo AC, Wahl RL. In vitro assessment of 2-fluoro-2-D-glucose, L-methionine, thymidine as agents to monitor the early response of a human adenocarcinoma cell line to radiotherapy. J Nucl Med 1993; 34:773–779.
21. Kubota K, Ishiwata K, Kubota R, et al. Tracer feasibility for monitoring tumor radiotherapy: a quadruple tracer study with fluorine-18-fluorodeoxyglucose or fluorine-18-fluorodeoxyuridine,L-[methyl-^{14}C] methionine, [6-^{3}H]thymidine, and gallium-67. J Nucl Med 1991; 32:2118–2123.
22. Minn H, Clavo AC, Grenman R, Wahl RL. In vitro comparison of cell proliferation kinetics and uptake of tritiated fluorodeoxyglucose andL-methionine in squamous-cell carcinoma of the head and neck. J Nucl Med 1'995; 36:252–258.
23. Stern PH, Hoffman RM. Elevated overall rates of transmethylation in cell lines from diverse human tumors. In Vitro 1984; 20:663–670.
24. Stern PH, Wallace CD, Hoffman RM. Altered methionine metabolism occurs in all members of a set of diverse human tumor cell lines. J Cell Physiol 1984; 119:29–34.
25. Wheatley DN. On the problem of linear incorporation of amino acids into cell protein. Experientia 1982; 38:818–820.
26. Weiss SW. WHO international histological classification of tumours. Histological typing of soft tissue tumours, 2nd edn. Berlin Heidelberg New York: Springer, 1994.
27. Langstrom B, Antoni G, Gullberg P, et al. Synthesis ofL-and D-[methy-^{11}C]methionine. J Nucl Med 1987; 19:1037–1040.
28. Leskinen-Kallio S, Nagren K, Lehikoinen P, Ruotsalainen U, Joensuu H. Uptake of^{11}C-methionine in breast cancer studied by PET. An association with the size of S-phase fraction. Br J Cancer 1991; 64:1121—1124.
29. Munzenrider JE, Liebsch NJ. Proton therapy for tumors of the skull base. Strahlenther Onkol 1999;175(Suppl 2):57–63.
30. Hug EB, Loredo LN, Slater JD, et al. Proton radiation therapy for chordomas and chondrosarcomas of the skull base. J Neurosurg 1999; 91:432–439.
31. Verstraete KL, Lang P. Post-therapeutic magnetic resonance imaging of bone tumors. Top Magn Reson Imaging 1999; 10:237–246.
32. Fletcher BD. Effects of pediatric cancer therapy on the musculoskeletal system. Pediatr Radiol 1997; 27:623–636.
33. Murphy WA Jr. Imaging bone tumors in the 1990s. Cancer 1991; 67:1169–1176.
34. Hawkins DS, Rajendran JG, Conrad EU 3rd, Bruckner JD, Eary JF. Evaluation of chemotherapy response in pediatric bone sarcomas by [F-18]-fluorodeoxy-D-glucose positron emission tomography. Cancer 2002; 94:3277–3284.
35. Findlay M, Young H, Cunningham D, et al. Noninvasive monitoring of tumor metabolism using fluorodeoxyglucose and positron emission tomography in colorectal cancer liver metastases: correlation with tumor response to fluorouracil. J Clin Oncol 1996; 14:700–708.
36. Muhr C, Gudjonsson O, Lilja A, Hartman M, Zhang ZJ, Langstrom B. Meningioma treated with interferon-alpha, evaluated with [^{11}C]-L-methionine positron emission tomography. Clin Cancer Res 2001; 7:2269—2276.
37. Andersson T, Wilander E, Eriksson B, Lindgren PG, Oberg K. Effects of interferon on tumor tissue content in liver metastases of human carcinoid tumors. Cancer Res 1990; 50:3413—3415.

Available online at www.sciencedirect.com
SCIENCE DIRECT®
Schizophrenia Research 69 (2004) 189–201
SCHIZOPHRENIA RESEARCH
www.elsevier.com/locate/schres

A polydiagnostic and dimensional comparison of epileptic psychoses and schizophrenia spectrum disorders

Masato Matsuura[a,*], Naoto Adachi[b], Yasunori Oana[c], Yoshiro Okubo[d], Masaaki Kato[e], Takashi Nakano[f], Noriyoshi Takei[g]

[a] *Department of Neuropsychiatry, Surugadai Nihon University Hospital, School of Medicine, 1-8-13 Surugadai, Kanda, Chiyoda, Tokyo 101-0062, Japan*
[b] *Adachi Mental Clinic, Sapporo, Japan*
[c] *Saint Paul Hospital, Tokyo, Japan*
[d] *Department of Medical Health, Tokyo Medical and Dental University, Tokyo, Japan*
[e] *National Center Hospital for Mental, Nervous and Muscular Disorders, Tokyo, Japan*
[f] *Department of Neuropsychiatry, Dokkyo Medical University, Tochigi, Japan*
[g] *Department of Neuropsychiatry, Hamamatsu Medical University, Shizuoka, Japan*

Received 21 June 2002; accepted 27 October 2002

Available online 25 February 2003

Abstract

After establishing the validity of the Japanese version of the Operational Criteria Checklist for Psychotic Illness (OPCRIT), we applied it to 58 consecutive patients with epileptic psychoses (index group) and to age- and sex-matched controls with schizophrenia spectrum disorders (control group). Compared with the control group, the index group had a low family history of schizophrenia, high premorbid personality disorder and unemployment, abrupt or acute onset of psychosis, good recovery with single or multiple episodes, and low deterioration from a premorbid level of function. From 9% to 52% of the index group and 38% to 84% of the control group were diagnosed with schizophrenia according to the operational criteria used. The percentages of patients diagnosed with schizophrenia based on various diagnostic criteria in the two groups were similar. In the index group, a diagnosis of schizophrenia was more commonly made among patients with inter-ictal psychosis than among those with post-ictal psychosis. An exploratory factor analysis identified five factor solutions of manic, negative, depressive, vegetative, and positive symptoms. Although positive and negative factor values were lower in the index group than in the control group, the two groups shared a similar factor profile. These results indicate that the difference in symptomatology between the two groups was quantitative rather than qualitative.

Keywords: OPCRIT; Polydiagnostic approach; Dimensional approach; Schizophrenia; Epileptic psychoses; Inter-ictal psychosis

1. Introduction

In light of the wide range of schizophrenic symptoms exhibited at various stages of epileptic psychoses, it has been suggested that no distinction can be made

* Corresponding author. Tel.: +81-3-3293-1711x311; fax: +81-3-3293-1733.
E-mail address: matsuura@med.nihon-u.ac.jp (M. Matsuura).

0920-9964/$ - see front matter © 2003 Elsevier B.V. All rights reserved.
doi:10.1016/S0920-9964(02)00492-9

from true schizophrenia on phenomenological grounds alone (Slater et al., 1963). On the other hand, some argue that epileptic psychoses can be distinguished on the basis of retention of normal affect response and/or the presence of peculiar personality traits, such as obstinacy, aggressiveness, and egocentricity (Matsuura and Trimble, 2000). We suggest that both arguments—that schizophrenia is always characterized by a blunted, deteriorated affect and that epileptic psychoses are always characterized by obstinacy and egocentricity—suffer from the substantial degree of ambiguity that is inherent in current diagnostic procedures for both epileptic psychoses and schizophrenia.

The practice of defining psychiatric disorders operationally became widely accepted in psychiatry following the introduction of the St. Louis criteria (Feighner et al., 1972) and the Research Diagnostic Criteria (RDC) (Spitzer et al., 1975) in the 1970s. After the incorporation of operational definitions in the Diagnostic and Statistical Manuals (DSM-III, American Psychiatric Association, 1980; DSM-III-R, American Psychiatric Association, 1987) of the American Psychiatric Association, operational criteria became general guidelines for clinicians in the 1980s for generating a diagnosis. This was followed by an operationalized version of the International Classification of Disease (ICD-10 (World Health Organization, 1992)). Explicit operationalized criteria are designed to be easily applied, with the rationale being to ensure high inter-rater reliability.

However, we suggest that problems still exist in the diagnosis of epileptic psychoses using these modern operational criteria. The first problem concerns the assumption that the etiology is either organic or functional. In most cases of epilepsy with psychotic disorders, the etiologic relationship between the psychoses and the epilepsy itself is not clear. In the diagnostic systems of the DSM-III-R and the ICD-10, the presence of epilepsy automatically leads to a diagnosis of "organic mental disorders," thereby precluding a diagnosis of functional disorders, such as schizophrenia, even if all required criteria are met (Trimble, 1991). The DSM-IV (American Psychiatric Association, 1994) has abandoned the term "organic" on the grounds that using the term would imply that some primary disorders might otherwise have a "non-organic" basis. Nonetheless, DSM-IV still requires clinicians to judge whether a disorder is "primary" or "due to a general medical condition". In addition, the use of subcategories of organic mental disorders (DSM-III-R and ICD-10) or mental disorders due to general medical conditions (DSM-IV) makes it difficult to capture the symptomatic complexity of and to specify the etiological heterogeneity of epileptic psychoses. This is because there are an insufficient number of categories for generating an accurate model of the illness. Therefore, we suggest that the dichotomy between organic or functional should be shelved for the time being in order to create a more representative series of distinctions.

The second problem of applying operational criteria to the categorization of epileptic psychoses is that there are several sets of different diagnostic criteria for schizophrenia. These different criteria do not always agree with one another. Some criteria are highly restrictive, whereas others are broad. Narrow and restrictive criteria of schizophrenia inevitably result in many "waste basket" categories, such as "psychotic disorder not otherwise specified (NOS)" and "atypical psychosis", which have little therapeutic value. Therefore, the simultaneous application of different diagnostic criteria may be needed.

The third problem with operational diagnostic criteria is that they impose upon clinicians a "top-down" diagnostic scheme, which is a rather rigid system. The absence of standardized severity ratings for a particular symptom within the criteria can mean that a mild self-limiting psychosis and a severe life-threatening one are included within the same diagnostic category (Matsuura et al., 2000). A dimensional method using a "bottom-up" approach has the advantage of being able to identify the entire array of symptoms that a patient may present as well as the severity of the individual symptoms (Van Os et al., 1999).

The Operational Criteria Checklist for Psychotic Illness (OPCRIT) (McGuffin et al., 1991) provides a polydiagnostic categorical and dimensional approach by dividing diagnostic criteria into their component items. It includes 90 items dealing with symptoms and demographic background information, and each item is defined in the glossary. Ratings are entered into the OPCRIT program which generate diagnoses for the main categories of affective and psychotic disorders defined according to eight major classification systems: St. Louis criteria (Feighner et al., 1972), Taylor and Abrams' criteria (Taylor and Abrams, 1978), RDC

(Spitzer et al., 1975), DSM-III (American Psychiatric Association, 1980), French classification (Pichot, 1984), DSM-III-R (American Psychiatric Association, 1987), ICD-10 (World Health Organization, 1992), and DSM-IV (American Psychiatric Association, 1994). There are two additional classifications—Schneider's first-rank symptoms (Schneider, 1959) and Carpenter's criteria (Carpenter et al., 1973)—which are for schizophrenia only. Three other criteria are for sub-typing classifications of schizophrenia (Tsuang and Winokur, 1974; Crow, 1980; Farmer et al., 1984).

The original version of the OPCRIT was shown to have excellent reliability between the three raters for 54 case vignettes (McGuffin et al., 1991). Excellent reliability in an international study including 30 clinicians for 30 case vignettes was also demonstrated (Williams et al., 1996). It provides a convenient, reliable, rapid, and valid approach to polydiagnostic assessment that can be used as an alternative to the conventional best-estimate consensus diagnostic procedures (Craddock et al., 1996; Azevedo et al., 1999). It has been used in a wide variety of clinical, epidemiological, and biological research applications.

The present multi-center study examines the differences and/or similarity in symptomatology of epileptic psychoses, which are supposed to be "organic", and of schizophrenia spectrum disorders, which are regarded as "functional", from a polydiagnostic categorical approach as well as a dimensional approach using the OPCRIT system.

2. Methods

The former version of OPCRIT (McGuffin et al., 1991) was introduced and translated into Japanese by one of the authors. We translated the new 3.4 version of OPCRIT into Japanese. All six authors are neuropsychiatrists with certifications in clinical psychiatry and epileptology. All attended an initial training and completed the Japanese version of OPCRIT (J-OPCRIT) independently on standard practice sets of 16 case vignettes with epileptic psychoses.

Thereafter, the multi-center study was conducted at six hospitals with specialized epilepsy clinics in and around Tokyo during 2001. These hospitals included one national center hospital, two public university hospitals, two private university hospitals, and one private mental hospital. The J-OPCRIT was applied to all consecutive patients with epileptic psychoses who were treated by one of the six authors at the hospitals within a 12-month study period. It was also applied to age- and sex-matched patients with schizophrenia spectrum disorders who were also treated by the same authors at the same hospital within the study period. An attempt has not been made to select particular forms of psychoses.

For completing the J-OPCRIT system, information on lifetime psychopathology was derived from a clinical interview with the patient, discussion with family members, and a review of the patient's medical records. The inclusion criteria included those patients who received a diagnosis of psychoses after the onset of epilepsy. Epilepsy was diagnosed based on the ILAE definition (Commission on Classification and Terminology of the ILAE, 1989). Psychoses are defined by the presence of hallucinations, delusions, or a limited number of several behavioral abnormalities, such as gross excitement and overactivity, marked psychomotor retardation, and catatonic behavior (World Health Organization, 1992). The exclusion criterion was the presence of consciousness disturbance during psychoses, comorbidity with senile dementia, personal history of alcohol abuse, or severe head trauma after the onset of epilepsy.

The inter-rater agreement was calculated by the range of kappa coefficients between two raters. The differences in demographic and clinical data of the two groups were statistically tested by a one-way analysis of variance (ANOVA) for parametric data and by chi-square test or by Fisher's exact probability test for categorical data. Exploratory factor analysis followed by varimax rotation was carried out using 60 symptom items of J-OPCRIT. The number of factors to be included was defined by the evaluation of the eigenvalue function, with factors with eigenvalues greater than average and without an abrupt change on the slope of the eigenvalue.

3. Results

3.1. Assessment of Japanese version of OPCRIT

Inter-rater agreement among the six raters showed that 24 items of clinical symptoms (pressured speech,

incoherent, thoughts racing, loss of pleasure, excessive self-reproach, diminished libido, suicidal ideation, diurnal variation, excessive sleep, weight loss, increased appetite, weight gain, increased sociability, increased self-esteem, grandiose delusions, delusions and hallucinations lasting for 1 week, persecutory/jealous delusions and hallucinations, thought insertion, thought withdrawal, thought broadcast, delusions of guilt, delusions of poverty, nihilistic delusions, thought echo) and six items of demographic information (family history of schizophrenia, family history of other psychiatric disorder, alcohol/drug abuse within 1 year of onset, alcohol/drug abuse/dependence with psychopathology, life time diagnosis of alcohol/drug abuse, impairment/incapacity during disorder) had a kappa range over 0.9.

Another 17 symptomatic items (bizarre behaviour, reckless activity, catatonia, distractibility, positive formal thought disorder, negative formal thought disorder, blunted affect, elevated mood, middle insomnia, early morning waking, persecutory delusions, widespread delusions, delusions of passivity, primary delusional perception, third person auditory hallucinations, running commentary voices, abusive/accusatory/persecutory voices) and nine demographic items (lack of insight, deterioration from a premorbid level of function, psychotic symptoms respond to neuroleptics, unemployed, poor premorbid work adjustment, poor premorbid social adjustment, definite psychosocial stressor prior to onset, premorbid personality disorder, duration of illness in weeks) had a kappa range of 0.8–0.9.

Fourteen symptomatic items (excessive activity, slowed activity, reduced need for sleep, agitated activity, loss of energy/tiredness, speech difficult to understand, restricted affect, irritable mood, dysphoria, poor appetite, initial insomnia, well organized delusions, bizarre delusions, other primary delusions) and four items of demographic information (rapport difficult, relationship psychotic/affective symptoms, mode of onset, course of disorder) showed a kappa range of 0.7–0.8, and five symptomatic items (inappropriate affect, poor concentration, delusions of influence, non-affective auditory hallucinations, non-affective hallucination in any modality) had a kappa range of 0.6–0.7.

Five diagnostic criteria—the ICD-10, DSM-III-R, DSM-III, RDC, and St. Louis—showed a kappa range of 0.8–0.9. Two other criteria—the DSM-IV and the French classification—had a kappa range of 0.7–0.8. The remaining system—Taylor and Abrams—showed a kappa range of 0.6–0.7. Therefore, the inter-rater agreement of the individual items as well as that of operational diagnoses of J-OPCRIT was satisfactory.

3.2. Demographic and clinical background (Table 1)

The index group was composed of 58 patients with epileptic psychoses (23 males, 35 females). The average age was 39.3 ± 12.5 years, the average onset of epilepsy was at 12.2 ± 8.4, and the average onset of psychoses was at 29.9 ± 10.5 years. There was almost an equal number of temporal lobe epilepsy (31 cases) and non-temporal lobe epilepsies (localization-related epilepsies in 22 cases and generalized epilepsies in five cases). Conventional hospital diagnoses were inter-ictal psychosis in 36 cases, post-ictal psychosis in 14 cases, and alternative psychosis in eight cases (Table 1).

The control group was composed of 58 age- and sex-matched patients with schizophrenia spectrum disorders. The average age was 39.0 ± 13.0 years, and the average age at onset of psychoses was 24.6 ± 10.6 years. Most of the conventional hospital diagnoses of the control group were schizophrenia, and the other diagnoses were schizotypal disorder, schizo-affective psychosis, and delusional disorder. Although the two groups were matched for age and sex, the average age at the onset of psychoses was higher in the index group than in the control group.

There was a striking difference in the presence of family history of schizophrenia, i.e., none in the index group and 21% in the control group. Compared with the schizophrenia spectrum disorder group, the epileptic psychosis group was characterized by the presence of premorbid personality disorder and of unemployment, and an abrupt or acute onset of psychoses. The prognosis was also significantly different. Good recovery with single or multiple episodes was seen in 53% among the index group and in 17% among the control group. The median duration of psychotic episodes was 8 weeks in the index group and 12 weeks in the control group. Chronic continuous course was seen in 36% in the index group and 52% in the control group, and deterioration from a premorbid level of function was found in 19% and 57%, respectively. The two groups

Table 1
Demographic and clinical background of the subjects

	Epileptic psychoses	Schizophrenia spectrum disorders
Number of cases (male, female)	58 (23, 35) cases	58 (23, 35) cases
Age	39.3 ± 12.5 years	39.0 ± 13.0 years
Age at onset of epilepsy	12.2 ± 8.4 years	
Type of epilepsy		
Temporal lobe epilepsy	31 cases	
Non-temporal lobe partial epilepsy	22	
Generalized epilepsy	5	
Conventional diagnosis		
Inter-ictal psychoses	36 cases	Schizophrenia 43 cases
Post-ictal psychosis	14	Schizotypal disorder 4
Alternative psychosis	8	Schizo-affective psychosis 3
		Delusional disorder 3
Age of onset of psychosis#	29.9 ± 10.5 years	24.6 ± 10.6 years
Family history of schizophrenia**	0 cases	12 cases
Family history of other psychiatric disorder	4 cases	3 cases
Premorbid personality disorder**	17 cases	5 cases
Unemployed*	18 cases	9 cases
Mode of onset**		
Abrupt onset (within hours or days)	18 cases	5 cases
Acute onset (within 1 week)	10	9
Acute onset (within 1 month)	18	9
Gradual onset (up to 6 months)	8	16
Insidious onset	4	19
Deterioration from premorbid level of function**	11 cases	33 cases
Psychotic symptoms respond to neuroleptics	37 cases	40 cases
Course of disorder**		
Single episode with good recovery	12 cases	2 cases
Multiple episodes with good recovery	19	8
Multiple episodes with partial recovery	6	18
Continuous chronic illness	20	23
Continuous chronic illness with deterioration	1	7

# $p<0.05$ (ANOVA).
* $p<0.05$ (chi-square test/ Fisher's exact probability test).
** $p<0.01$ (chi-square test/ Fisher's exact probability test).

were similar in terms of the number of patients with a family history of other psychiatric disorders and the response rate to neuroleptic treatments of psychotic symptoms.

3.3. Distribution of operational diagnostic classification (Table 2)

The St. Louis definition for schizophrenia was the most restrictive, and only 10% of patients in the index group and 38% in the control group were diagnosed with schizophrenia. The definitions of schizophrenia based on the French classification system and the DSM-III were also restrictive, and a diagnosis of schizophrenia was made for 9% and 12% of patients in the index group and 41% and 45% in the control group, respectively. The DSM-IV, DSM-III-R, and RDC criteria were relatively narrow, and a diagnosis of schizophrenia was made for 24%, 26%, and 53% in the index group and 59%, 66%, and 66% in the control group, respectively. The ICD-10 criteria for schizophrenia were almost identical with a conventional hospital diagnosis and 47% in the index group and 76% in the control group were diagnosed with schizophrenia. Taylor and Abrams' criteria were the broadest, and a diagnosis of schizophrenia was made for 52% in the index group and 84% in the control group. The RDC revealed no

Table 2
Percentage of the distributions of operational diagnosis

		Epileptic psychoses	Schizophrenia spectrum disorders
Full criteria	St. Louis criteria (1972)**		
	definite/probable schizophrenia	10%	38%
	others	90	62
	RDC (1978)		
	narrow/broad schizophrenia	53%	66%
	schizo-affective disorder	10	19
	unspecified functional psychosis	31	14
	affective disorder with psychosis	5	2
	Taylor and Abrahams' classification (1978) **		
	schizophrenia	52%	84%
	others	48	16
	DSM-III (1980)**		
	schizophrenia	12%	45%
	atypical psychosis	64	43
	schizophreniform disorder	7	5
	affective disorder with psychosis	5	5
	paranoid disorder	12	2
	French classification (1987)**		
	chronic schizophrenia	9%	41%
	delusional attack	17	17
	interpretive psychosis	0	3
	chronic hallucinatory psychosis	2	2
	bouffee delirante	16	0
	others	57	36
	DSM-III-R (1987)**		
	schizophrenia	26%	66%
	atypical psychosis	26	19
	schizophreniform disorder	26	9
	schizoaffective disorder	5	5
	delusional disorder	17	2
	ICD-10 (1993)**		
	paranoid/undifferentiated schizophrenia	47%	76%
	affective disorder with psychosis	3	3
	others	50	21
	DSM-IV (1994)**		
	schizophrenia	24%	59%
	psychotic disorder not otherwise specified	34	28
	schizophreniform disorder	19	9
	delusional disorder	17	2
	schizoaffective disorder	5	3
For schizophrenia only	Schneider's first rank symptoms (1959)**		
	schizophrenia with first-rank symptoms	34%	48%
	others	66	52
	Carpenter's classification (1976)		
	'level 5/6' schizophrenia	76%	71%
	others	24	29
For schizophrenia subtyping	Tsung and Winokur subtypes (1974)**		
	undifferentiated schizophrenia	69%	50%
	hebephrenic schizophrenia	10	38
	paranoid schizophrenia	22	12
	Crow subtypes (1980)**		
	type I	78%	26%
	mixed type	22	74